Journal of Hydrology 521 (2015) 470–481

Contents lists available at ScienceDirect

Journal of Hydrology

journal homepage: www.elsevier.com/locate/jhydrol

Controls of soil hydraulic characteristics on modeling groundwater recharge under different climatic conditions

Tiejun Wang [a,*], Trenton E. Franz [a], Vitaly A. Zlotnik [b]

[a] School of Natural Resources, University of Nebraska–Lincoln, Hardin Hall, 3310 Holdrege Street, Lincoln, NE 68583, USA
[b] Department of Earth and Atmospheric Sciences, University of Nebraska–Lincoln, 214 Bessey Hall, Lincoln, NE 68588, USA

ARTICLE INFO

Article history:
Received 28 October 2014
Received in revised form 15 December 2014
Accepted 16 December 2014
Available online 25 December 2014
This manuscript was handled by Corrado Corradini, Editor-in-Chief, with the assistance of Aldo Fiori, Associate Editor

Keywords:
Groundwater recharge
Climatic conditions
Vadose zone model
Soil hydraulic characteristics

SUMMARY

To meet the challenge of estimating spatially varying groundwater recharge (*GR*), increasing attention has been given to the use of vadose zone models (VZMs). However, the application of this approach is usually constrained by the lack of field soil hydraulic characteristics (SHCs) required by VZMs. To tackle this issue, SHCs based on the van Genuchten or Brooks–Corey model are generally estimated by pedotransfer functions or taken from texture based class averages. With the increasing use of this method, it is important to elucidate the controls of SHCs on computing *GR* mostly due to the high nonlinearity of the models. In this study, it is hypothesized that the nonlinear controls of SHCs on computing *GR* would vary with climatic conditions. To test this hypothesis, a widely used VZM along with two SHCs datasets for sand and loamy sand is used to compute *GR* at four sites in the continental Unites States with a significant gradient of precipitation (*P*). The simulation results show that the distribution patterns of mean annual *GR* ratios ($\overline{GR}/\overline{P}$, where $\overline{GR}$ and $\overline{P}$ are mean annual *GR* and *P*, respectively) vary considerably across the sites, largely depending on soil texture and climatic conditions at each site. It is found that $\overline{GR}/\overline{P}$ is mainly controlled by the shape factor n in the van Genuchten model and the nonlinear effect of n on $\overline{GR}/\overline{P}$ varies with climatic conditions. Specifically, for both soil textures, the variability in $\overline{GR}/\overline{P}$ is smallest at the Andrews Forest with the highest $\overline{P}$ (191.3 cm/year) and $\overline{GR}/\overline{P}$ is least sensitive to n; whereas, the variability in $\overline{GR}/\overline{P}$ at the Konza Prairie ($\overline{P}$ = 84.2 cm/year) is the largest and $\overline{GR}/\overline{P}$ is most sensitive to n. With further decreasing $\overline{P}$, the nonlinear effect of n weakens at the Barta Brothers ($\overline{P}$ = 57.3 cm/year) and Sevilleta ($\overline{P}$ = 20.3 cm/year), leading to smaller $\overline{GR}/\overline{P}$ variability at those two sites than at the Konza Prairie. The results also reveal that $\overline{GR}/\overline{P}$ in finer soils with smaller n values decreases more rapidly with decreasing $\overline{P}$.

1. Introduction

Groundwater recharge (*GR*) is an important process in terrestrial hydrological cycles. Knowledge of *GR* and its spatial distribution is critical for closing groundwater balance equations and for assessing sustainable use of groundwater resources (Scanlon et al., 2006). However, the complex dependence of recharge processes on various affecting factors (e.g., soil, climate, topography, landscape position, and vegetation) precludes accurate estimates of *GR* as it may vary substantially across landscapes (Scanlon et al., 2002; Kim and Jackson, 2012). Although a range of physical, chemical, and isotopic techniques have been developed over the past several decades to estimate *GR* (Lerner et al., 1990; Allison et al., 1994; Scanlon et al., 2002), increasing attention has been given to the use of process-based vadose zone models (VZMs) for estimating spatially varying *GR* due to the cost and time efficiency of the method (Keese et al., 2005; Small, 2005; Wang et al., 2009a; Le Coz et al., 2013; Ibrahim et al., 2014).

Application of VZMs for calculating *GR* requires soil hydraulic characteristics (SHCs), which are usually unavailable for needed spatial resolutions. To overcome this problem, a general practice is to apply SHCs estimated from pedotransfer functions (PTF) to obtain *GR* at large spatial scales (Keese et al., 2005; Small, 2005; Faust et al., 2006; Wang et al., 2009a). Pedotransfer functions are used to convert easily obtainable or readily available soil properties to SHCs (Schaap et al., 2001; Wösten et al., 2001). For instance, Small (2005) analyzed the climatic controls on *GR* in the Southwestern US using a 1-D VZM with mean SHCs, and revealed that the occurrence of *GR* was significantly affected by rainfall characteristics. Also based on a 1-D VZM, Keese et al. (2005) evaluated the spatial distribution of *GR* in Texas by employing the Rosetta

* Corresponding author.
E-mail address: twang3@unl.edu (T. Wang).

http://dx.doi.org/10.1016/j.jhydrol.2014.12.040
0022-1694/

program (Schaap et al., 2001) to estimate SHCs. The authors found that *GR* was higher in sandy soils under bare surface conditions, and could be reduced by factors of 2–11 for finer-textured soils and by factors of 2–30 under vegetated conditions. Moreover, PTF-estimated SHCs have been recently used for simulating various land surface processes (Gutmann and Small, 2007; Decharme et al., 2011; Wood et al., 2011).

Despite the advantages of utilizing PTF-estimated SHCs, the reliability of such approaches might be problematic due to the uncertainties in the SHCs estimates (Schaap and Leij, 1998; Schaap et al., 2001), the nonlinear nature of subsurface flow systems (Wang et al., 2009a), and soil heterogeneity (Hohenbrink and Lischeid, 2014). Faust et al. (2006) calculated catchment-scale *GR* and showed that computed *GR* might vary by an order of magnitude depending on the choice of PTFs. By applying a VZM, Wang et al. (2009a) calculated *GR* in a semiarid region based on three SHCs datasets, and showed that the use of mean SHCs for obtaining representative *GR* values had caveats and generalizations to other climatic regimes were not apparent. In particular, future *GR* projections require a thorough understanding of the SHCs uncertainty impacts on *GR* calculations under different climatic conditions (Green et al., 2011; Taylor et al., 2013).

In this study, we hypothesize that the controls of SHCs on *GR* calculations are dependent on climatic conditions. To illustrate our hypothesis, Fig. 1 shows a group of soil water retention curves based on the van Genuchten model (van Genuchten, 1980), which were derived from the UNSODA soil database for loamy sand (Nemes et al., 2001). It can be seen from Fig. 1 that near the wet end of the retention curves (e.g., -10 cm), the variations in the curves are smaller than in the intermediate range (e.g., -100 cm), which might lead to less impacts of SHCs uncertainties on modeling *GR* under very wet conditions. Similarly, the uncertainty impacts of SHCs on modeling *GR* would be also smaller under very dry conditions as demonstrated by the dry end of the retention curves (e.g., -1000 cm) in Fig. 1. Thus, one can expect that the controls of SHCs on *GR* calculations would be climate-dependent.

To test our hypothesis without the need to generate synthetic hydrometeorological data (e.g., Small, 2005), four research sites located in the continental United States with a significant precipitation (P) gradient were selected to analyze the controls of SHCs on modeling *GR* under different climatic conditions. To be consistent with previous modeling studies (Small, 2005; Wang et al., 2009a), two SHCs datasets for sand and loamy sand were chosen to represent the variability in SHCs. Daily hydrometeorological data from each site were used to drive a 1-D VZM for computing *GR*. In addition, both bare surface and vegetated conditions were

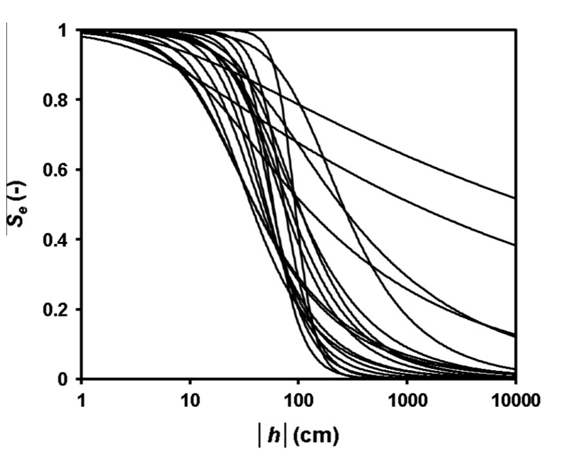

Fig. 1. Relationships between effective saturation degree (S_e) and water pressure head (h) for loamy sand derived from the UNSODA soil database (Nemes et al., 2001).

considered to examine the effect of vegetation on *GR* distributions. For the vegetated condition, remotely sensed data and literature values of physiological parameters were adopted. Finally, the controls of SHCs on *GR* distributions were analyzed using histograms as well as a sensitivity analysis of *GR* to different van Genuchten parameters.

2. Methods and materials

2.1. Flow model

A widely used 1-D VZM, Hydrus-1D (Šimunek et al., 2005) was chosen in this study due to the accuracy of its numerical algorithm (Zlotnik et al., 2007). The Hydrus-1D model can simulate 1-D vertical soil moisture flow in porous media by solving the Richards equation:

$$\frac{\partial \theta}{\partial t} = \frac{\partial}{\partial x}[K(h)(\frac{\partial h}{\partial x}) - K(h)] - S(h) \tag{1}$$

where θ [L^3/L^3] is volumetric moisture content, t [T] is time, x [L] is spatial coordinate (positive downward), h [L] is pressure head, K [L/T] is hydraulic conductivity, and S [1/T] is root water uptake.

The van Genuchten model (Mualem, 1976; van Genuchten, 1980) was used to describe the constitutive relations among θ, h, and K:

$$\theta(h) = \begin{cases} \theta_r + \frac{\theta_s - \theta_r}{(1+|\alpha h|^n)^m}, & h < 0 \\ \theta_s \quad h \geqslant 0 \end{cases} \tag{2}$$

$$K(h) = K_S \times S_e^l \times \left[1 - (1 - S_e^{1/m})^m\right]^2 \tag{3}$$

where θ_r [L^3/L^3] is residual moisture content, θ_s [L^3/L^3] is saturated moisture content, K_S [L/T] is saturated hydraulic conductivity, $S_e = (\theta - \theta_r)/(\theta_s - \theta_r)$ is effective saturation degree, and α, n, and l are shape factors: α [1/L] is inversely related to air entry pressure, n [–] is a measure of pore size distribution, and l [–] is a lumped parameter accounting for pore tortuosity and connectivity, and $m = 1 - 1/n$.

A standard atmospheric upper boundary condition was adopted in this study (Neuman et al., 1974), which can switch from a prescribed flux to a prescribed head boundary condition when limiting pressure heads are exceeded. Surface runoff (without ponding) was allowed to occur when P exceeded soil infiltration capacity (e.g., K_S) or soil was saturated. The other option in the Hydrus-1D model with ponding (e.g., the maximum ponding depth = 0.5 cm) was also evaluated. It was shown that the inclusion of ponding did not affect the conclusions made in this study, and therefore the results are not analyzed here. At the lower boundary, a unit hydraulic gradient condition was applied (Keese et al., 2005; Small, 2005; Wang et al., 2009a). Accordingly, *GR* is defined here as the amount of water leaving the lower boundary. The length of simulated soil columns was 5 m with 501 nodes evenly distributed between the surface and bottom. Numerical experiments showed that additional spatial nodes did not improve the model performance.

In this study, *GR* was computed for both vegetated and bare surface conditions to examine the impact of vegetation on the *GR* distributions. For the bare surface condition, potential evapotranspiration (ET_p) was set to be equal to potential soil evaporation (E_p). For the vegetated condition, ET_p was partitioned between potential transpiration (T_p) and E_p based on Beer's law (Ritchie, 1972):

$$E_p(t) = ET_p(t) \times e^{-k \times \mathrm{LAI}(t)} \tag{4}$$

$$T_p(t) = ET_p(t) - E_p(t) \tag{5}$$

where k is an extinction coefficient set to be 0.5 and LAI is leaf area index. The sink term $S(h)$ in Eq. (1) was simulated according to Feddes et al. (1978):

$$S(h) = \beta(h) \times S_p \tag{6}$$

where $\beta(h)$ [–] is a dimensionless function and varies between 0 and 1 depending on soil matric potentials, and S_p [1/T] is potential root water uptake and assumed to be equal to T_p. The distribution of $S_p(x)$ over the root zone is based on root density distributions.

2.2. Hydrometeorological and physiological data

At four research sites in the continental US, the Hydrus-1D model was forced by observed daily hydrometeorological data that spanned over five years. Among those sites, three were taken from the Long Term Ecological Research (LTER) Network, including Andrews Forest (AF, 44°13′N, 122°23′W), Konza Prairie (KP, 39°05′N, 96°35′W), and Sevilleta (SV, 34°21′N, 106°53′W). The last site was located at the University of Nebraska's Barta Brothers (BB) Ranch experimental site in the eastern Nebraska Sand Hills (42°14′N, 99°39′W). The detailed information on those sites can be found elsewhere (http://www.lternet.edu/; Wang et al., 2008, 2009b). The Penman–Monteith equation (Allen et al., 1998) was used to calculate daily ET_p. Mean monthly ET_p and P at each site are plotted in Fig. 2, and the summary of mean annual ET_p ($\overline{ET_p}$) and P ($\overline{P}$) are given in Table 1. Except for the AF, the other three sites exhibited similar climate seasonality. Therefore, to ensure the applicability of the conclusions made in this study, the effect of the seasonality at the AF on GR distributions was also evaluated (see the following section for details).

To partition daily ET_p into E_p and T_p, LAI data were retrieved from the MODIS_MOD15A2 dataset (Myneni et al., 2002), which has a spatial resolution of 1 km × 1 km at 8-day intervals. Based on the procedure of Wang and Zlotnik (2012), a 3 km × 3 km grid cell window, which was centered at each site according to their geographical locations, was used to extract LAI data from the MOD15A2 dataset. The resulting nine LAI values were then averaged and daily LAI data at each site were finally obtained by linear interpolation between the 8-day averaged LAI values. To simulate root water uptake, the root density distribution at the BB (e.g., grass) was selected based on field data reported by Wang et al. (2009b). For the other three sites (e.g., forest at the AF, grass at the KP, and shrub at the SV), the root density distributions were based on values given by Jackson et al. (1996). Literature values of physiological parameters used by the Feddes et al. (1978) model were also adopted (Wesseling, 1991; Gutiérrez-Jurado et al., 2006; Vogel et al., 2013).

Since the initial conditions were unknown, all of the simulations were repeated for four times (e.g., 20 years in total) until the soil moisture profiles were in equilibrium with climatic forcings to minimize the effects of initial conditions on GR calculations (Small, 2005; Wang et al., 2009a). Groundwater recharge calculated from the last repetition is used in the following analyses.

Table 1
Mean annual precipitation ($\overline{P}$), potential evapotranspiration ($\overline{ET_p}$), and aridity index ($\overline{ET_p}/\overline{P}$) at different research sites.

	$\overline{P}$ (cm/year)	$\overline{ET_p}$ (cm/year)	$\overline{ET}/\overline{P}$ (-)
Andrews Forest	191.3	81.9	0.43
Konza Prairie	84.2	122.6	1.46
Barta Brothers	57.3	172.8	3.01
Sevilleta	20.3	160.6	7.92

2.3. SHCs datasets

To be consistent with previous modeling studies (Small, 2005; Wang et al., 2009a), GR for sand and loamy sand were simulated in this study. Two SHCs datasets were used to represent the differences in SHCs (Nemes et al., 2001; Wang et al., 2009a). The first dataset was taken from the UNSODA database (Nemes et al., 2001) and included measured SHCs (referred to as a measured

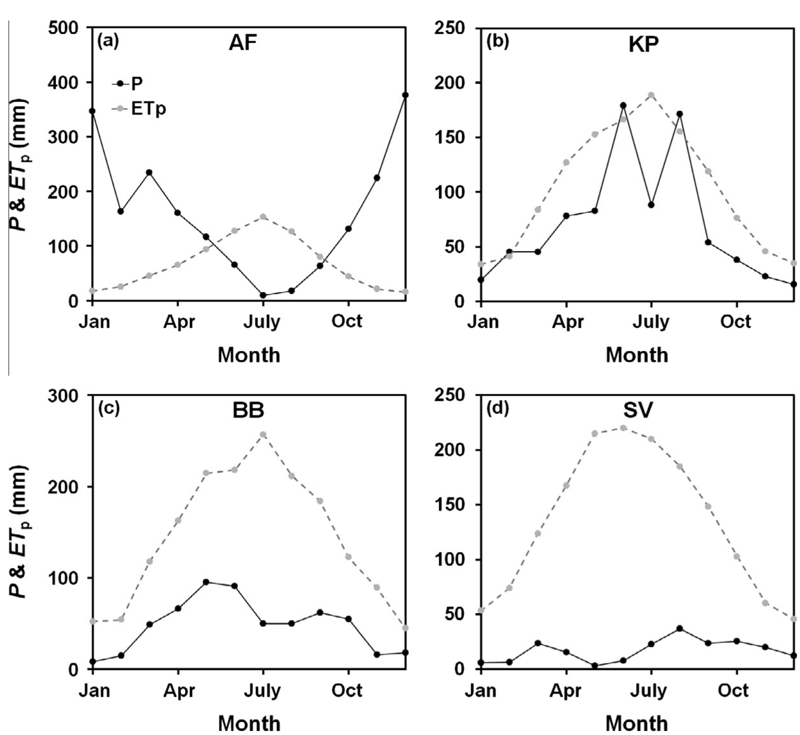

Fig. 2. Mean monthly precipitation (P) and potential evapotranspiration (ET_p) during the simulation periods at (a) Andrews Forest (AF), (b) Konza Prairie (KP), (c) Barta Brothers (BB), and (d) Sevilleta (SV).

dataset hereafter). The UNSODA database has been widely used in PTF-related studies (e.g., Schaap and Leij, 2000; Gutmann and Small, 2007). For this dataset, 51 samples for sand and 19 samples for loamy sand were retrieved from the UNSODA database with complete sets of measured van Genuchten parameters. Due to the limited sample sizes in the measured dataset, a second dataset with correlated SHCs generated by Wang et al. (2009a) was adopted (referred to as a correlated dataset hereafter) and a brief overview of the correlated dataset is given here. The correlated dataset was derived from the measured dataset by computing mean values of the van Genuchten parameters (e.g., θ_r, θ_s, $\log_{10}\alpha$, $\log_{10}n$, $\log_{10}K_S$, and l) and a co-variance matrix for those parameters. A Monte-Carlo procedure by Carsel and Parrish (1988) was then used to draw new samples with correlated SHCs from the co-variance matrix and mean values. A total of 100 generated samples for both sand and loamy sand were used in this study to have more complete *GR* distributions. The statistical summary of the parameter values for the measured and correlated datasets is reported in Table 2.

3. Results and discussions

3.1. Distribution patterns of GR under different climatic and surface conditions

There were significant differences in $\overline{P}$ across the four selected sites from 191.3 cm/year at the AF to 20.3 cm/year at the SV, resulting in a wide range of aridity indices (Table 1). Therefore, to compare *GR* distributions at different sites, mean annual *GR* ratios ($\overline{GR}/\overline{P}$, where $\overline{GR}$ is mean annual *GR*) are used in the following analyses. Owing to the use of long spin-up periods (i.e.,

Table 2
Statistical summary of the measured and correlated datasets on soil hydraulic characteristics.

Soil texture	Dataset	N	θ_r (cm^3/cm^3)		θ_s (cm^3/cm^3)		$\log_{10}\alpha$ (1/cm)		$\log_{10}n$ (–)		$\log_{10}K_s$ (cm/day)		l (–)	
			Mean	σ	Mean	σ	Mean	σ	Mean	σ	Mean	σ	Mean	σ
Sand	Measured	51	0.048	0.036	0.379	0.046	−1.512	0.308	0.464	0.223	2.544	0.732	−0.149	1.532
	Correlated	100	0.059	0.032	0.380	0.047	−1.481	0.306	0.479	0.186	2.617	0.593	0.057	1.121
Loamy Sand	Measured	19	0.061	0.041	0.418	0.069	−1.493	0.364	0.308	0.174	2.275	0.619	−0.680	3.146
	Correlated	100	0.060	0.033	0.416	0.062	−1.525	0.320	0.300	0.154	2.374	0.524	0.076	2.328

σ: standard deviation.

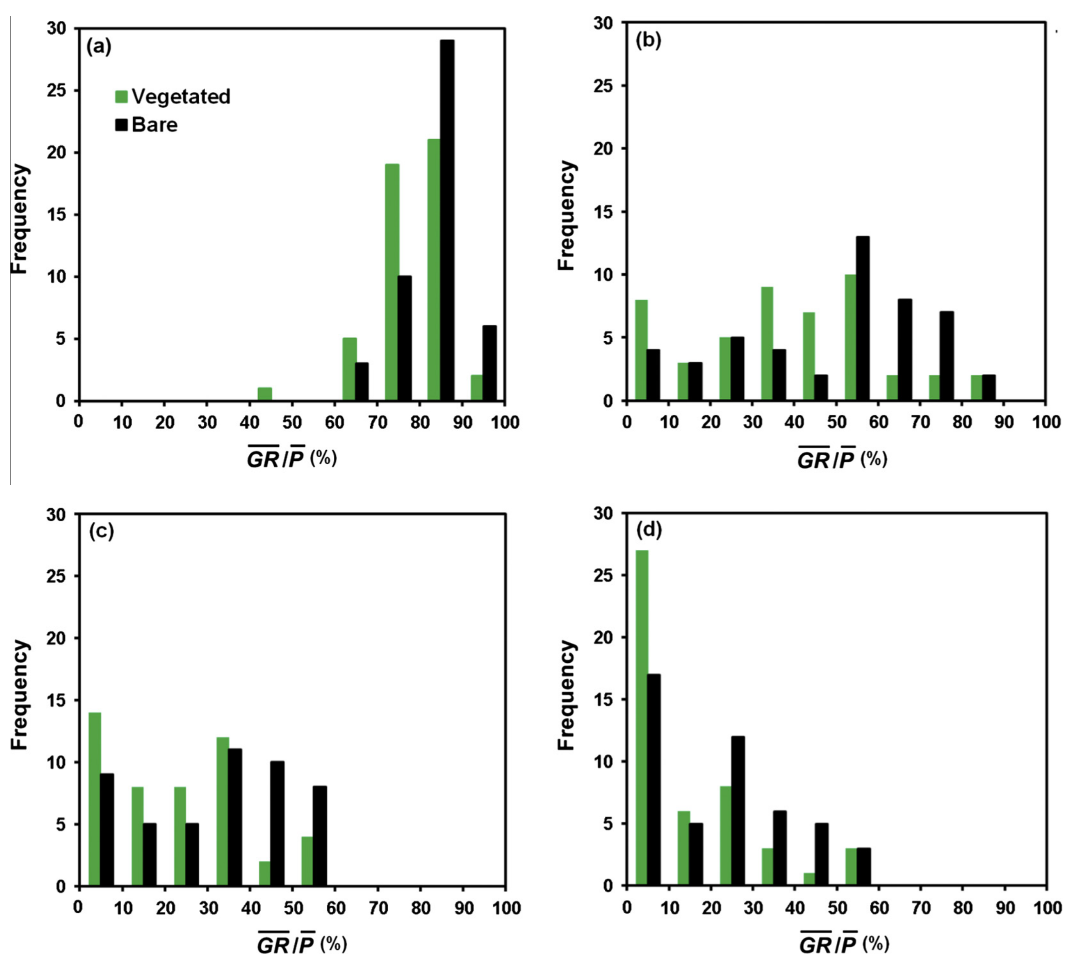

Fig. 3. Distributions of mean annual groundwater recharge ratios ($\overline{GR}/\overline{P}$) under different surface conditions for sand based on the measured dataset at (a) Andrews Forest, (b) Konza Prairie, (c) Barta Brothers, and (d) Sevilleta. Bin size is 10%.

15 years) for the simulations, the change in soil moisture storage had a negligible effect on GR calculations. In addition, over 95% of the simulations showed that surface runoff was less than 1% in the water balance calculations, and thus it is not analyzed here. Note that for the measured dataset, three simulations for sand and five simulations for loamy sand were removed from the analyses due to large mass balance errors (>2%), which were caused by low negative values of the parameter l in the van Genuchten model (Schaap and Leij, 2000; Wang et al., 2009a), particularly for the SV with very dry climatic conditions.

For both bare surface and vegetated conditions, the histograms of $\overline{GR}/\overline{P}$ derived from the measured dataset are shown in Fig. 3 for sand (denoted as $\overline{GR_S}/\overline{P}$) and in Fig. 4 for loamy sand (denoted as $\overline{GR_{LS}}/\overline{P}$). It can be seen from Fig. 3 that the distribution patterns of $\overline{GR_S}/\overline{P}$ varied considerably among the sites under both surface conditions, mainly due to the contrasts in climatic conditions among the sites. Under the bare surface condition and for the same set of SHCs, the $\overline{GR_S}/\overline{P}$ value was highest at the AF with the wettest climate as indicated by the highest $\overline{P}$ and lowest aridity index. All $\overline{GR_S}/\overline{P}$ ratios at the AF exceeded 60%. As the climate became drier (e.g., increasing aridity index and decreasing $\overline{P}$) from the KP to the SV, $\overline{GR_S}/\overline{P}$ progressively decreased for the same set of SHCs. As an illustration, the number of simulations (a total of 100 at each site) with $\overline{GR_S}/\overline{P}$ ratios less than 10% increased from 4 at the KP to 9 at the BB and 17 at the SV (Fig. 3). Meanwhile, the range of the $\overline{GR_S}/\overline{P}$ distribution was narrowest at the AF (63.4–91.9%) with the majority of simulated $\overline{GR_S}/\overline{P}$ ratios concentrated around a peak, indicating the smallest variability in the $\overline{GR_S}/\overline{P}$ distribution and the least sensitivity of $\overline{GR_S}/\overline{P}$ to SHCs variations. By comparison, the spread of the $\overline{GR_S}/\overline{P}$ distribution at the KP (2.3–80.5%) was widest, suggesting the largest sensitivity of $\overline{GR_S}/\overline{P}$ to SHCs variations. With a drier climate, the range of the $\overline{GR_S}/\overline{P}$ distribution gradually became smaller again at the BB (0.2–59.8%) and the SV (0.2–53.0%).

Owing to the fact that root can extract deeper soil moisture for transpiration, $\overline{GR_S}/\overline{P}$ became smaller under the vegetated condition (Fig. 3), which is consistent with previous modeling results (e.g., Keese et al., 2005). However, even with the consideration of vegetation, the differences in $\overline{GR_S}/\overline{P}$ distributions (e.g., their ranges) at different sites remained similar to the one under the bare surface condition. At the AF, except for one simulation with $\overline{GR_S}/\overline{P} = 49.0\%$, the rest of the $\overline{GR_S}/\overline{P}$ ratios exceeded 60% (66.1–90.9%). The range of $\overline{GR_S}/\overline{P}$ at the KP was largest (0.3–81.0%), and became smaller again at the BB (0.2–57.3%) and the SV (0–52.8%).

Despite the smaller sample size for loamy sand, the ranges and shapes of the $\overline{GR_{LS}}/\overline{P}$ distributions also varied substantially across different sites under both bare surface and vegetated conditions. Similar to the results for sand, the $\overline{GR_{LS}}/\overline{P}$ value at the AF (71.8–86.7% for bare surface, and 69.4–84.3% for vegetated surface) was highest for the same set of SHCs among the four sites; whereas, the range of the $\overline{GR_{LS}}/\overline{P}$ distribution at the KP (9.3–63.7% for bare surface, and 3.4–56.2% for vegetated surface) was largest. Moreover, the ranges of the $\overline{GR_{LS}}/\overline{P}$ distributions at the BB (0.3–44.6% for bare surface, and 0–38.0% for vegetated surface) and the SV (0.2–33.4% for bare surface, and 0–27.5% for vegetated surface) were also smaller than the ones at the KP. Note that the minimum value of $\overline{GR_S}/\overline{P}$ at each site was generally smaller than the one for $\overline{GR_{LS}}/\overline{P}$ due to the larger variability in SHCs for sand as shown in the following section (see Figs. 8 and 9). Nonetheless, Figs. 3 and 4

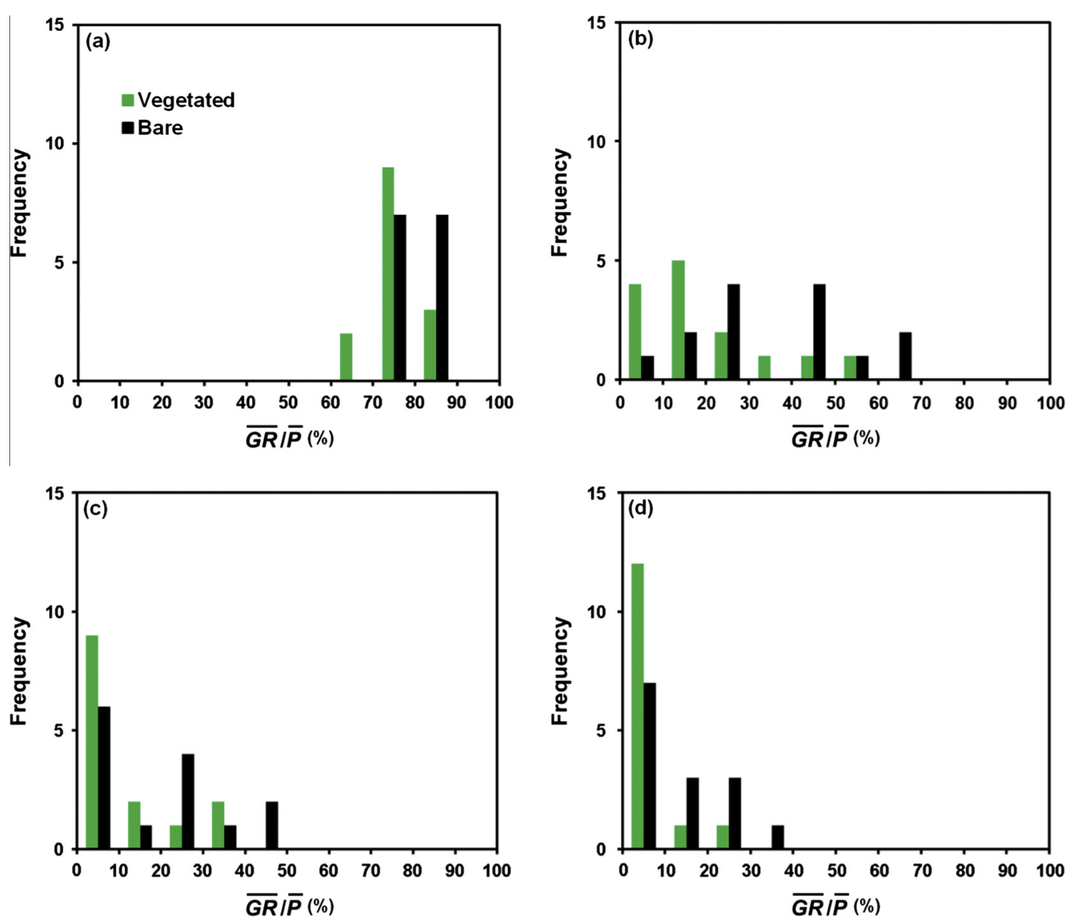

Fig. 4. Distributions of mean annual groundwater recharge ratios ($\overline{GR}/\overline{P}$) under different surface conditions for loamy sand based on the measured dataset at (a) Andrews Forest, (b) Konza Prairie, (c) Barta Brothers, and (d) Sevilleta. Bin size is 10%.

demonstrate that the controls of SHCs on *GR* calculations are climate-dependent.

On the basis of soil texture, average values of SHCs for each soil class are widely used to calculate representative *GR* values at spatial scales greater than point scales (Small, 2005; Gutmann and Small, 2007; Decharme et al., 2011). The values of $\overline{GR}/\overline{P}$ calculated from average values of SHCs (Table 2) are reported in Table 3 for both vegetated and bare surface conditions. As expected, $\overline{GR_S}/\overline{P}$ was larger than $\overline{GR_{LS}}/\overline{P}$ at each site for the same conditions, which is consistent with the conclusions made in previous modeling studies that coarser soils generally lead to higher *GR* (Keese et al., 2005; Small, 2005). However, there were significant overlaps between $\overline{GR_S}/\overline{P}$ and $\overline{GR_{LS}}/\overline{P}$ distributions at each site (Figs. 3 and 4). This is because unlike soil texture that is only defined by particle size distributions, SHCs are also influenced by other soil factors, such as bulk density, organic matter, and pore size distribution (Schaap et al., 2001; Wösten et al., 2001; Wang et al., 2009b), which leads to overlaps of parameter space of SHCs (e.g., see Figs. 8 and 9 for an illustration) and thus the overlaps of $\overline{GR_S}$ and $\overline{GR_{LS}}$ distributions. Furthermore, the wide spreads of $\overline{GR_S}/\overline{P}$ and $\overline{GR_{LS}}/\overline{P}$ distributions from the simulation results here demonstrate that *GR* computed solely based on mean SHCs or soil textural information is unlikely to capture the general characteristics of *GR* distributions at larger spatial scales, regardless of climatic conditions. Therefore, caution should be used when using average values of SHCs for obtaining regional representations of *GR* values.

Table 3
Summary of mean annual groundwater recharge ratios (%) calculated based on mean values of soil hydraulic characteristics from the measured dataset.

Location	Sand		Loamy sand	
	Bare surface	Vegetated surface	Bare	Vegetated surface
Andrews Forest	88.18	84.82	81.42	78.36
Konza Prairie	68.90	59.24	43.58	33.12
Barta Brothers	48.67	39.63	24.57	15.75
Sevilleta	37.75	28.69	10.56	3.17

To have a more complete view of the $\overline{GR}/\overline{P}$ distributions, the simulation results, including bare surface and vegetated conditions, from the correlated dataset are plotted in Fig. 5 for sand and in Fig. 6 for loamy sand. As expected, the shapes of the $\overline{GR}/\overline{P}$ distributions under the same surface condition differed significantly at different sites, depending on climatic conditions and soil texture. More importantly, Figs. 5 and 6 illustrate that the variations in the $\overline{GR}/\overline{P}$ distributions were consistent with the results from the measured dataset: the KP exhibited the largest ranges of the $\overline{GR}/\overline{P}$ distribution for both sand and loamy sand. To further illustrate the controls of SHCs on the variability in $\overline{GR}/\overline{P}$ under different climatic conditions, the standard deviations of $\overline{GR}/\overline{P}$ ($\sigma_{\overline{GR}/\overline{P}}$) along with $\overline{P}$ at each site are shown in Fig. 7 for the measured and correlated datasets. In general, regardless of soil texture and surface conditions, there existed an upward convex relationship between $\sigma_{\overline{GR}/\overline{P}}$ and $\overline{P}$. In particular, at the AF with a very humid climate, the standard deviations of $\overline{GR}/\overline{P}$ were significantly lower than the ones at the other three sites, which also indicated the least sensitivity of $\overline{GR}/\overline{P}$ to SHCs variations. At the KP with a subhumid climate, the standard deviations of $\overline{GR}/\overline{P}$ were largest among the

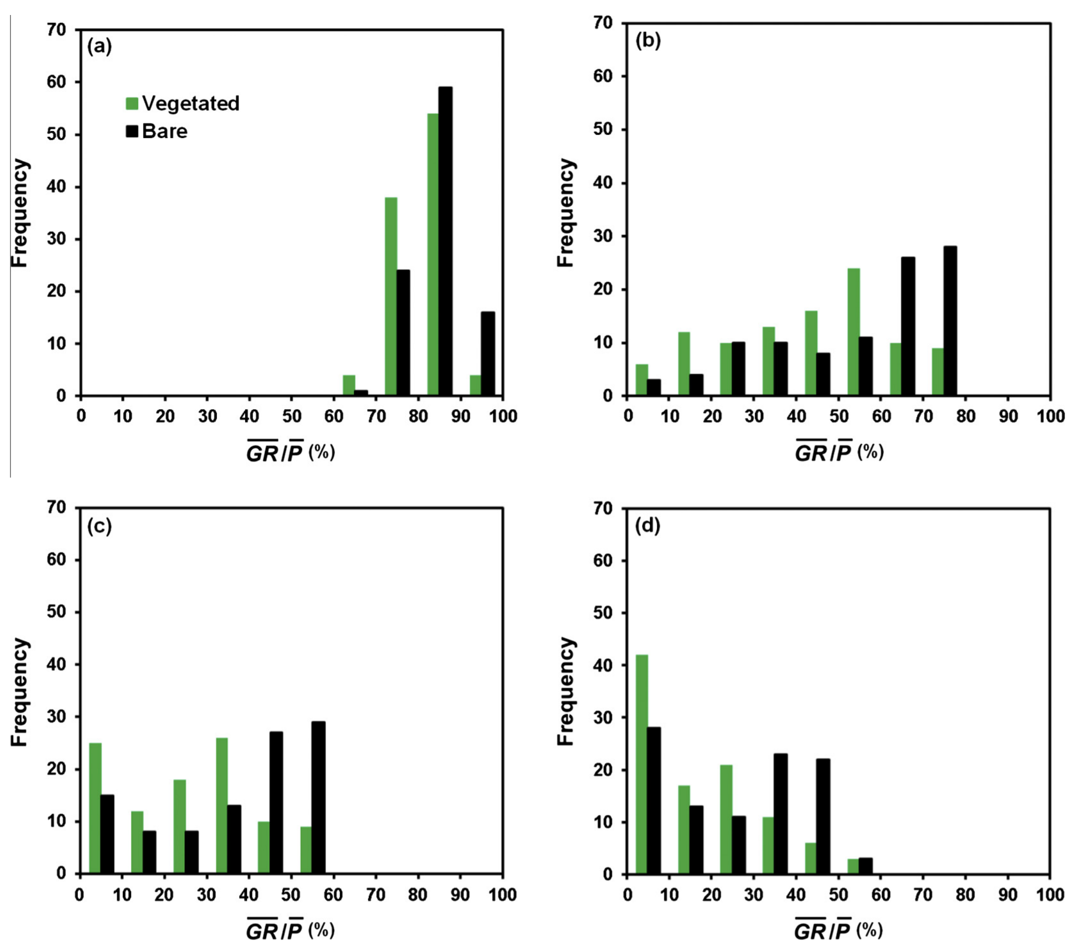

Fig. 5. Distributions of mean annual groundwater recharge ratios ($\overline{GR}/\overline{P}$) under different surface conditions for sand based on the correlated dataset at (a) Andrews Forest, (b) Konza Prairie, (c) Barta Brothers, and (d) Sevilleta. Bin size is 10%.

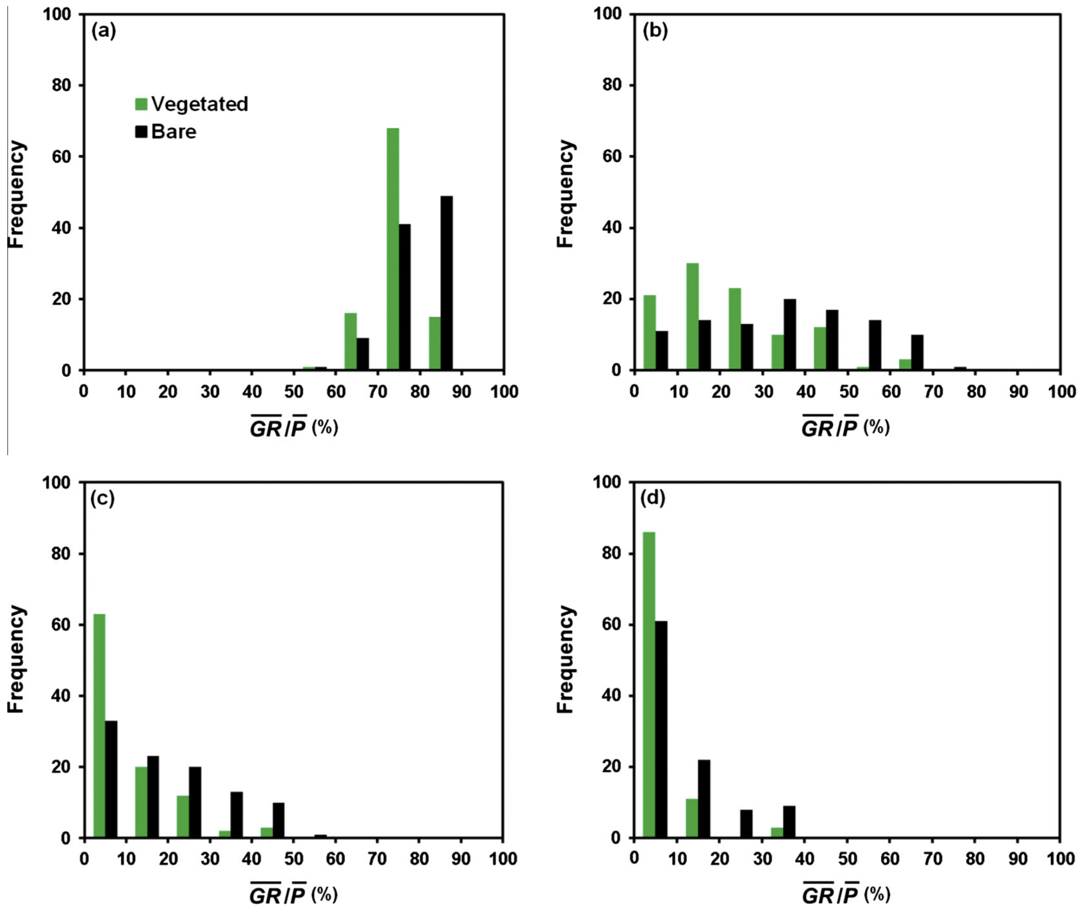

Fig. 6. Distributions of mean annual groundwater recharge ratios ($\overline{GR}/\overline{P}$) under different surface conditions for loamy sand based on the correlated dataset at (a) Andrews Forest, (b) Konza Prairie, (c) Barta Brothers, and (d) Sevilleta. Bin size is 10%.

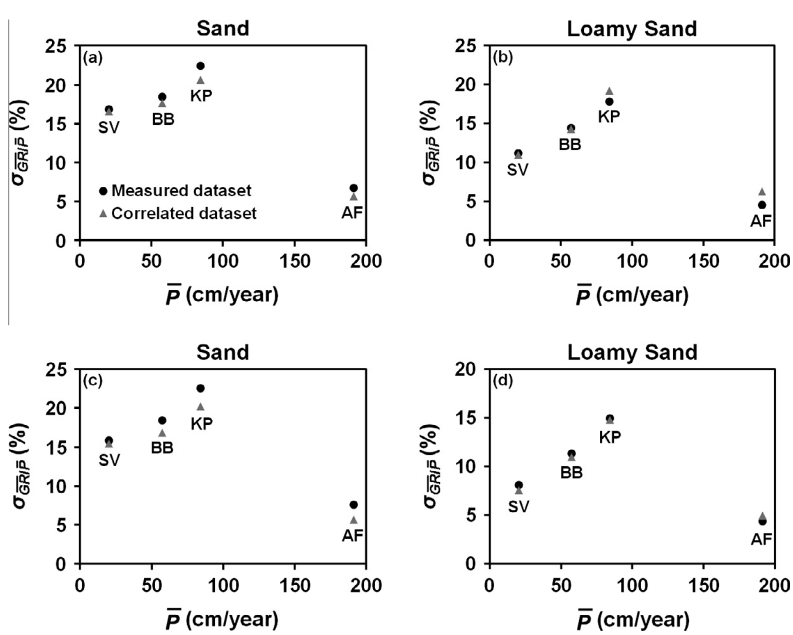

Fig. 7. Impacts of mean annual precipitation ($\overline{P}$) on standard deviations of mean annual groundwater recharge ratios ($\sigma_{\overline{GR}/\overline{P}}$) under bare surface (a and b) and vegetated (c and d) conditions.

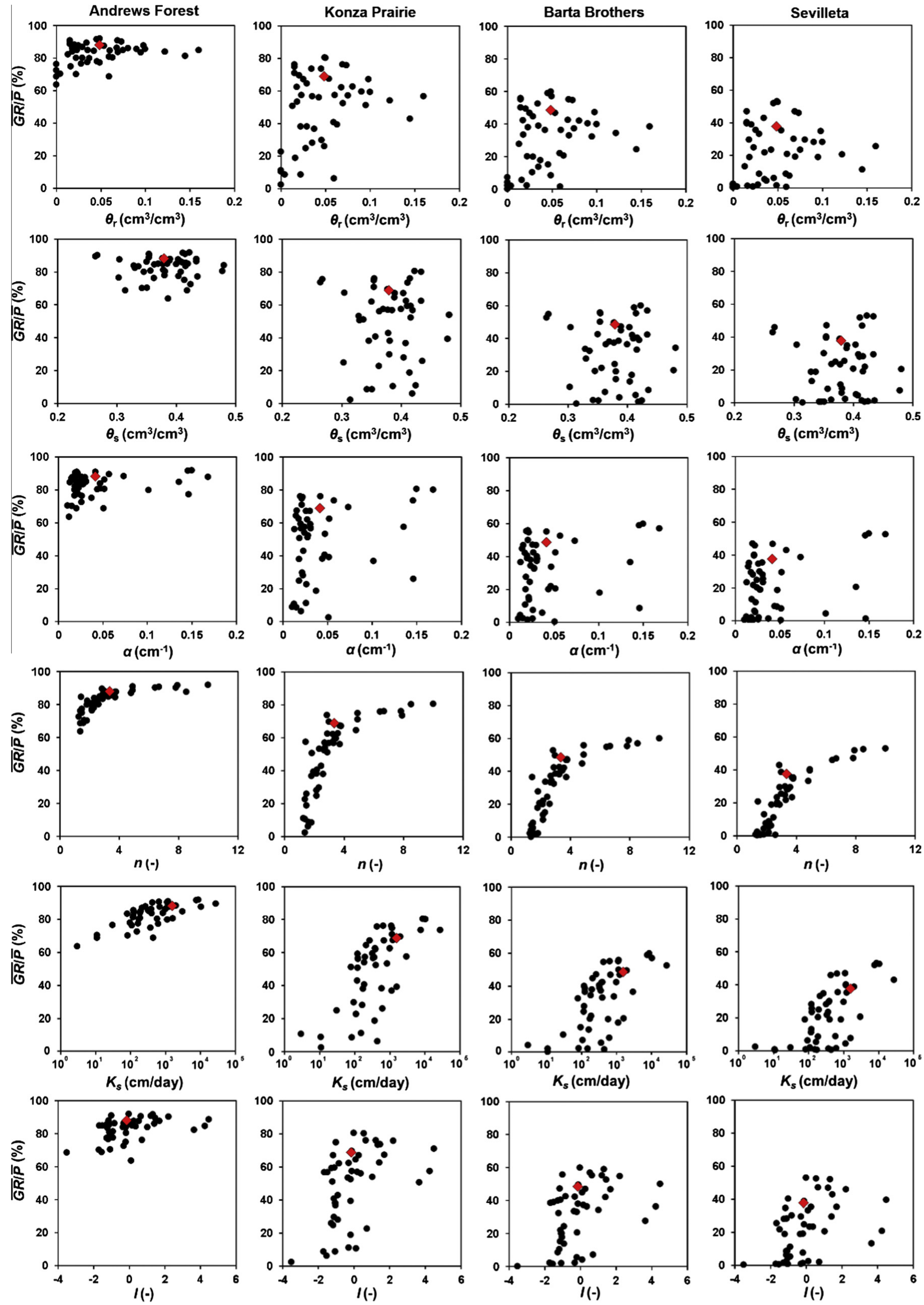

Fig. 8. Correlations between mean annual groundwater recharge ratios ($\overline{GR}/\overline{P}$) under the bare surface condition for sand and the van Genuchten parameters derived from the measured dataset. Red diamonds are $\overline{GR}/\overline{P}$ ratios based on mean values of SHCs. (For interpretation of the references to colour in this figure legend, the reader is referred to the web version of this article.)

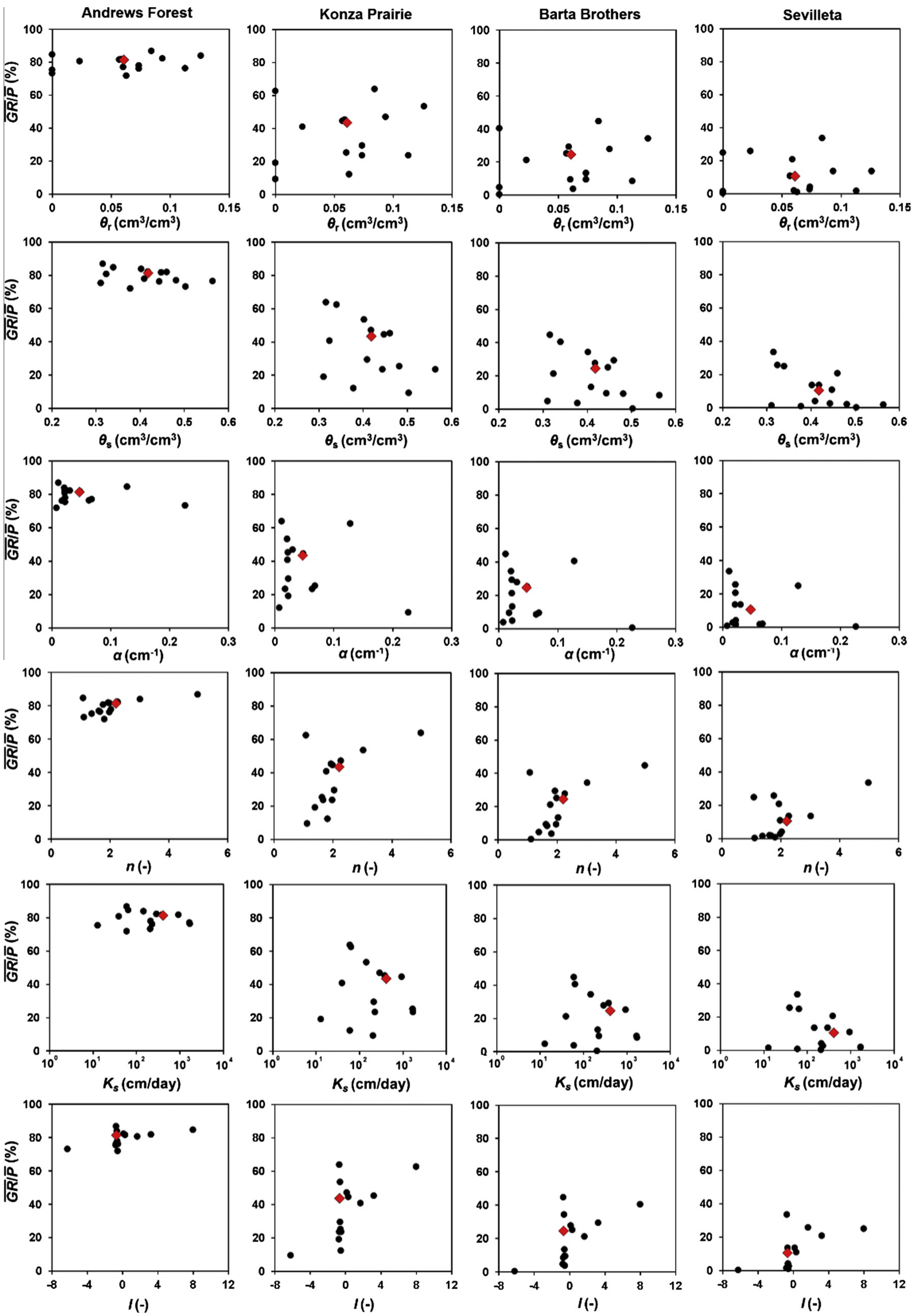

Fig. 9. Correlations between mean annual groundwater recharge ratios ($\overline{GR}/\overline{P}$) under the bare surface condition for loamy sand and the van Genuchten parameters derived from the measured dataset. Red diamonds are $\overline{GR}/\overline{P}$ ratios based on mean values of SHCs. (For interpretation of the references to colour in this figure legend, the reader is referred to the web version of this article.)

four sites. With a semiarid climate at the BB and an arid climate at the SV, the standard deviations of $\overline{GR}/\overline{P}$ begun to gradually decrease.

Although P and ET_p are the primary controls on actual evapotranspiration (ET_a) and thus GR, other factors (e.g., seasonality, vegetation, and rainfall characteristics) may also exert impacts on ET_a and GR (Zhang et al., 2001; Small, 2005; Yokoo et al., 2008; Wang et al., 2009c). It can be seen from Fig. 2 that the seasonality at the AF showed a different pattern than at the other three sites. To ensure the general applicability of the findings in this study, a hypothetical condition was also simulated for the AF by shifting daily P for 180 days. Therefore, P and ET_p were now in phase. The hypothetical simulations were carried out using the measured dataset under the vegetated condition. The resulting $\sigma_{\overline{GR}/\overline{P}}$ was 6.66% and 5.32% for sand and loamy sand, respectively. Those $\sigma_{\overline{GR}/\overline{P}}$ values were comparable to the ones shown in Fig. 7 for the AF, indicating that the seasonality at the AF played a minor role in affecting the variations in the $\overline{GR}/\overline{P}$ distributions. Overall, the simulation results corroborate our hypothesis that the controls of SHCs on GR calculations would vary with climatic conditions.

3.2. Controls of SHCs on GR calculations under different climatic conditions

Wang et al. (2009a) showed that GR in a semiarid region was mainly controlled by the shape factor n in the van Genuchten model. To investigate additional controls of SHCs on GR distributions under different climatic conditions, the relationships of $\overline{GR}/\overline{P}$ with the van Genuchten parameters are plotted in Fig. 8 for sand and in Fig. 9 for loamy sand. For the purpose of brevity, only the results under the bare surface condition are shown here for the measured dataset, but we note that the conclusions remain consistent when vegetation is included. Among all of the van Genuchten parameters, K_S, θ_s, and θ_r are physical parameters, while α, n, and l are fitting parameters that are indicators of different soil physical properties. In Fig. 8, there appeared to be no correlation of $\overline{GR_S}/\overline{P}$ with θ_s and θ_r at the four sites, while $\overline{GR_S}/\overline{P}$ was positively correlated with $\log_{10}K_S$. More interestingly, $\overline{GR_S}/\overline{P}$ was largely controlled by the shape factor n, which is a measure of pore size distribution. In general, $\overline{GR_S}/\overline{P}$ nonlinearly increased with increasing n until $\overline{GR_S}/\overline{P}$ reached a certain threshold, which was dependent on climatic conditions. Although the sample size was smaller for loamy sand, similar observations are also shown in Fig. 9, except for the correlation between $\overline{GR_{LS}}$ and $\log_{10}K_S$. In addition, the non-parametric Spearman's rank correlation test was conducted, and the correlation coefficients between $\overline{GR}/\overline{P}$ and different van Genuchten parameters are reported in Table 4. For sand, $\overline{GR_S}/\overline{P}$ was correlated with n, $\log_{10}K_S$, and l with n being the most important controlling factor. Although the correlation between $\overline{GR_{LS}}/\overline{P}$ and n for loamy sand was not statistically significant at $p = 0.05$, n was generally the leading controlling factor on $\overline{GR_{LS}}/\overline{P}$ (except for the SV), followed by l.

The dominant control of n on modeling various subsurface processes is also found in previous studies (e.g., Pollacco et al., 2008; Wang et al., 2009a; Hohenbrink and Lischeid, 2014; Wang, 2014). Physically, a larger n value indicates a coarser-textured soil, which results in higher GR. Mathematically, n mainly controls the shape of retention curves and affects GR through soil evaporation. As explained by Wang et al. (2009a), for a larger n, the decrease in hydraulic conductivity with decreasing soil moisture becomes stronger, which reduces the capability of the soil profile for transmitting soil moisture upwards to the surface for evaporation and thus leads to higher GR. Meanwhile, soils with smaller n values have larger capabilities to retain water in shallow soil depths against gravity. Thus, the infiltrated water is no longer available for evapotranspiration. Figs. 8 and 9 further reveal that the nonlinear control of n is also dependent on climatic conditions. Specifically, changes in n values had the least effect on computing GR at the AF with the smallest variation in the $\overline{GR}/\overline{P}$ distribution; whereas, the nonlinear control of n on the calculation of GR was strongest at the KP and $\overline{GR_S}/\overline{P}$ could change significantly with a small shift in the n value (e.g., the range between 1 and 4), indicating that the sensitivity of n in the calculation of GR was strongest at the AF. However, with drier climatic conditions at the BB and the SV, the nonlinear effect of n on the calculation of GR weakened, as evidenced in the gradually declining slopes of the $n - \overline{GR}/\overline{P}$ curves at the BB and the SV; as a result, the variations in the $\overline{GR}/\overline{P}$ distributions at those two sites were less than the one at the KP. Finally, the parameter l, which is a lumped factor accounting for pore tortuosity and connectivity, has a similar effect on soil moisture flux as n, but to a lesser degree. However, when the nonlinear control of n is weak (e.g., soils with smaller n values), the effect of l on computing GR may become important.

To further elucidate the control of n on GR calculations under different climatic conditions, and for the same set of SHCs, $\overline{GR}/\overline{P}$ values at the other three sites were normalized to the one at the AF (denoted as $\eta = (\overline{GR}/\overline{P})/(\overline{GR}/\overline{P})_{AF}$). The obtained results under the bare surface condition from the measured dataset are shown in Fig. 10 for sand and loamy sand. Compared to the relationships between n and $\overline{GR}/\overline{P}$ (Figs. 8 and 9), similar nonlinear relationships existed between n and η for both sand and loamy sand. When the climate shifted from wetter to drier conditions, GR in finer soils with smaller n values decreased more rapidly and thus was more responsive to decreasing $\overline{P}$. The results thus suggest that GR in regions with finer soils is more affected by climate changes in a relative term as indicated by the ratio of η in Fig. 10. Overall, based on the sensitivity analysis of $\overline{GR}/\overline{P}$ to various soil hydraulic parameters under different climatic conditions, the simulation results support our hypothesis that the controls of SHCs on the calculation of GR depends on climatic conditions.

Table 4
Spearman's rank correlation coefficients between van Genuchten parameters and mean annual groundwater recharge ratio under the bare surface condition for the measured dataset.

SHCs	Sand				Loamy sand			
	AF	KP	BB	SV	AF	KP	BB	SV
θ_r	0.269	0.275	0.272	0.276	0.267	0.294	0.258	0.135
θ_s	0.020	0.030	0.030	0.040	−0.275	−0.310	−0.332	−0.411
α	0.207	0.210	0.201	0.198	−0.055	−0.112	−0.200	−0.255
n	0.909**	0.901**	0.921**	0.905**	0.481	0.503	0.525	0.440
K_s	0.651**	0.667**	0.647**	0.625**	0.042	0.024	−0.011	−0.130
l	0.488**	0.541**	0.497**	0.535**	0.424	0.455	0.503	0.581*

* $p<0.05$.
** $p<0.01$.

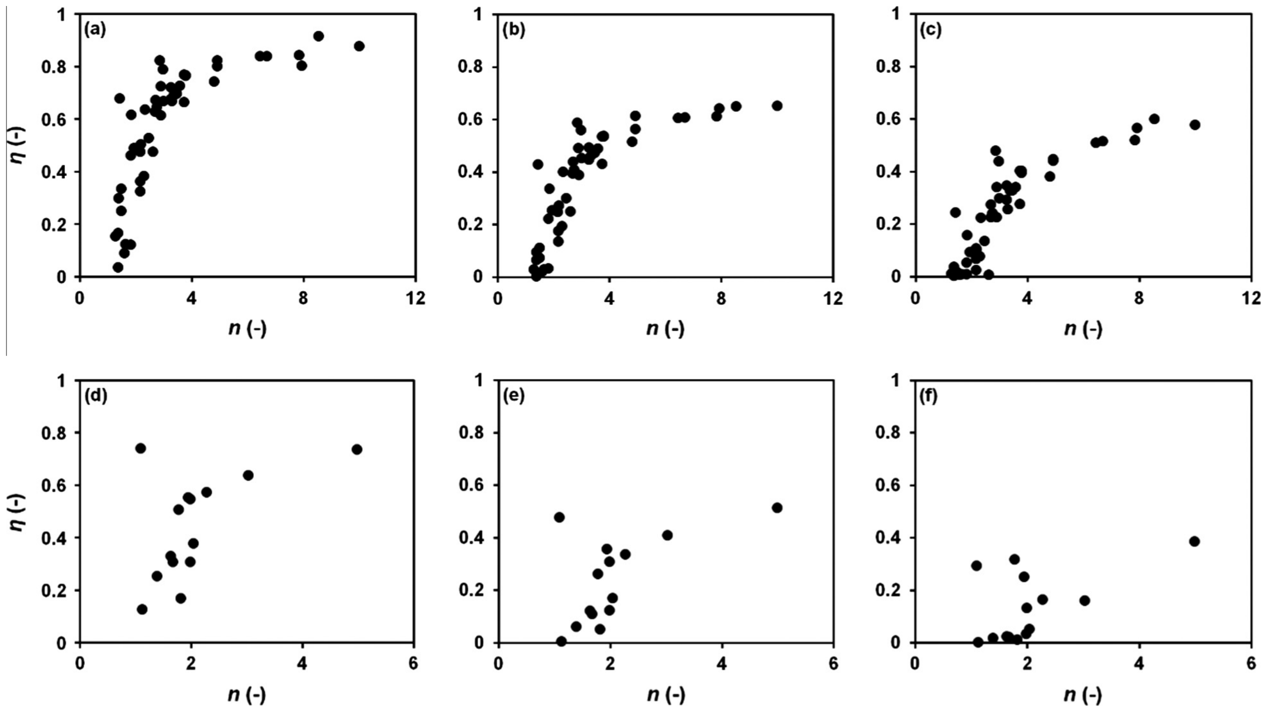

Fig. 10. Relationships between the shape factor n and normalized mean annual groundwater recharge ratios ($\overline{GR}/\overline{P}$) under the bare surface condition at Konza Prairie (a and d), Barta Brothers (b and e), and Sevilleta (c and f) with respect to the ones at Andrews Forest. η is the ratio of $\overline{GR}/\overline{P}$ at the other three sites over the one at Andrews Forest for the same set of SHCs (i.e., $\eta = (\overline{GR}/\overline{P})/(\overline{GR}/\overline{P}_{AF})$). Data shown in (a)–(c) and in (d)–(f) are derived from sand and loamy sand in the measured dataset, respectively.

4. Conclusions

The controls of soil hydraulic characteristics (SHCs) on groundwater recharge (*GR*) calculations were evaluated using a vadose zone modeling approach at four research sites located in the continental United States with significant differences in mean annual precipitation ($\overline{P}$) among those sites. Daily hydrometeorological data obtained from those sites along with two SHCs datasets were used in a 1-D vadose zone model for computing *GR*. In addition, both bare surface and vegetated conditions were considered. Our hypothesis that the controls of SHCs on *GR* calculations would vary with climatic conditions was supported by the simulation results. The distribution patterns of mean annual groundwater recharge ratios ($\overline{GR}/\overline{P}$) varied considerably across the sites, mainly depending on soil texture and climatic conditions. At the Andrews Forest with the highest $\overline{P}$, the variability in $\overline{GR}/\overline{P}$ was smallest, while the one at the Konza Prairie with intermediate $\overline{P}$ was the highest. With further decreases in $\overline{P}$, the variability in $\overline{GR}/\overline{P}$ decreased at the Barta Brothers and Sevilleta. This phenomenon indicates that the uncertainty impacts of SHCs on *GR* calculations vary with climatic conditions. The simulation results also showed that the distribution patterns of $\overline{GR}/\overline{P}$ were mainly controlled by the shape factor n, and the nonlinear relationship between $\overline{GR}/\overline{P}$ and n changed with climatic conditions. Moreover, $\overline{GR}/\overline{P}$ in finer soils with smaller n values decreased more rapidly with decreasing $\overline{P}$, suggesting that *GR* in regions with finer soils is proportionally more affected by changes in climatic conditions. Our simulation results have practical implications for modeling *GR* in regions with different climatic conditions, particularly with the increasing spatial resolution of land surface models.

Acknowledgments

The authors would like to thank the teams (M. Nelson from Andrews Forest, J. Blair from Konza Prairie, and S. Collins from Sevilleta) at the Long Term Ecological Research sites for making the hydrometeorological data accessible and the High Plain Regional Climate Center for providing the hydrometeorological data at the Barta Brothers ranch site. This study was partially funded by the Water for Food program of the University of Nebraska–Lincoln and the Cold Regions Research and Engineering Laboratory. We would also like to thank two anonymous reviewers for their constructive comments, which led to the improvements of this work.

References

Allen, R.G., Pereira, L.S., Raes, D., Smith, M., 1998. Crop evapotranspiration: Guidelines for computing crop water requirements. Irrig. Drain. Pap. 56, U.N. Food and Agric. Organ., Rome.

Allison, G.B., Gee, G.W., Tyler, S.W., 1994. Vadose-zone techniques for estimating groundwater recharge in arid and semiarid regions. Soil Sci. Soc. Am. J. 58, 6–14.

Carsel, R.F., Parrish, R.S., 1988. Developing joint probability distributions of soil water retention characteristics. Water Resour. Res. 24, 755–769.

Decharme, B., Boone, A., Delire, C., Noilhan, J., 2011. Local evaluation of the Interaction between soil biosphere atmosphere soil multilayer diffusion scheme using four pedotransfer functions. J. Geophys. Res. 116, D20126. http://dx.doi.org/10.1029/2011JD016002.

Faust, A.E., Ferré, T.P.A., Schaap, M.G., Hinnell, A.C., 2006. Can basin-scale recharge be estimated reasonably with water-balance models? Vadose Zone J. 5, 850–855. http://dx.doi.org/10.2136/vzj2005.0109.

Feddes, R.A., Kowalik, P.J., Neuman, S.P., 1978. Simulation of Field Water Use and Crop Yield. John Wiley and Sons, New York, NY.

Green, T.R., Taniguchi, M., Kooi, H., Gurdak, J.J., Allen, D.M., Hiscock, K.M., Treidel, H., Aureli, A., 2011. Beneath the surface of global change: impacts of climate change on groundwater. J. Hydrol. 405, 532–560. http://dx.doi.org/10.1016/j.jhydrol.2011.05.002.

Gutiérrez-Jurado, H.A., Vivoni, E.R., Harrison, J.B.J., Guan, H., 2006. Ecohydrology of root zone water fluxes and soil development in complex semiarid rangelands. Hydrol. Process. 20, 3289–3316.

Gutmann, E.D., Small, E.E., 2007. A comparison of land surface model soil hydraulic properties estimated by inverse modeling and pedotransfer functions. Water Resour. Res. 43, W05418. http://dx.doi.org/10.1029/2006WR005135.

Hohenbrink, T.L., Lischeid, G., 2014. Texture-depending performance of an in situ method assessing deep seepage. J. Hydrol. 511, 61–71.

Ibrahim, M., Favreau, G., Scanlon, B.R., Seidel, J.L., Le Coz, M., Demarty, J., Cappelaere, B., 2014. Long-term increase in diffuse groundwater recharge following expansion of rainfed cultivation in the Sahel, West Africa. Hydrogeol. J., 1–13.

Jackson, R.B., Canadell, J., Ehleringer, J.R., Mooney, H.A., Sala, O.E., Schulze, E.D., 1996. A global analysis of root distributions for terrestrial biomes. Oecologia 108, 389–411.

Keese, K.E., Scanlon, B.R., Reedy, R.C., 2005. Assessing controls on diffuse groundwater recharge using unsaturated flow modeling. Water Resour. Res. 41, W06010. http://dx.doi.org/10.1029/2004WR003841.
Kim, J.H., Jackson, R.B., 2012. A global analysis of groundwater recharge for vegetation, climate, and soils. Vadose Zone J. 11, 188–222.
Le Coz, M., Favreau, G., Ousmane, S.D., 2013. Modeling increased groundwater recharge due to change from rainfed to irrigated cropping in a semiarid region. Vadose Zone J. 12. http://dx.doi.org/10.2136/vzj2012.0148.
Lerner, D.N., Issar, A.S., Simmers, I., 1990. Groundwater Recharge, A Guide to Understanding and Estimating Natural Recharge. Rep. 8, 345 pp., Int. Assoc. of Hydrogeol., Kenilworth, U.K.
Mualem, Y., 1976. A new model for predicting the hydraulic conductivity of unsaturated porous media. Water Resour. Res. 12, 513–522.
Myneni, R.B., Hoffman, S., Knyazikhin, Y., Privette, J.L., Glassy, J., Tian, Y., Wang, Y., Song, X., Zhang, Y., Smith, Y., Lotsch, A., Friedl, M., Morisette, J.T., Votava, P., Nemani, R.R., Running, S.W., 2002. Global products of vegetation leaf area and fraction absorbed PAR from year one of MODIS data. Remote Sens. Environ. 83, 214–231.
Nemes, A., Schaap, M.G., Leij, F.J., Wösten, J.H.M., 2001. Description of the unsaturated soil hydraulic database UNSODA version 2.0. J. Hydrol. 251, 151–162.
Neuman, S.P., Feddes, R.A., Bresler, E., 1974. Finite Element Simulation of Flow in Saturated-Unsaturated Soils Considering Water Uptake by Plants. Third Annual Report, Project No. A10-SWC-77, Hydraulic Engineering Lab, Technion, Haifa, Israel.
Pollacco, J.A.P., Ugalde, J.M.S., Angulo-Jaramillo, R., Braud, I., Saugier, B., 2008. A linking test to reduce the number of hydraulic parameters necessary to simulate groundwater recharge in unsaturated soils. Adv. Water Resour. 31, 355–369.
Ritchie, J.T., 1972. Model for predicting evaporation from a row crop with incomplete cover. Water Resour. Res. 8, 1204–1213.
Scanlon, B.R., Healy, R.W., Cook, P.G., 2002. Choosing appropriate techniques for quantifying groundwater recharge. Hydrogeol. J. 10, 18–39. http://dx.doi.org/10.1007/s10040-001-0176-2.
Scanlon, B.R., Keese, K.E., Flint, A.L., Flint, L.E., Gaye, C.B., Edmunds, W.M., Simmers, I., 2006. Global synthesis of groundwater recharge in semiarid and arid regions. Hydrol. Process. 20, 3335–3370. http://dx.doi.org/10.1002/hyp.6335.
Schaap, M.G., Leij, F.J., 1998. Database-related accuracy and uncertainty of pedotransfer functions. Soil Sci. 163, 765–779. http://dx.doi.org/10.1097/00010694-199810000-00001.
Schaap, M.G., Leij, F.J., 2000. Improved predictions of unsaturated hydraulic conductivity with the Mualem–van Genuchten model. Soil Sci. Soc. Am. J. 64, 843–851.
Schaap, M.G., Leij, F.J., van Genuchten, M.T., 2001. ROSETTA: a computer program for estimating soil hydraulic parameters with hierarchical pedotransfer functions. J. Hydrol. 251, 163–176. http://dx.doi.org/10.1016/S0022-1694(01)00466-8.
Šimunek, J., van Genuchten, M.T., Sejna, M., 2005. The HYDRUS-1D Software Package for Simulating the One-Dimensional Movement of Water, Heat, and Multiple Solutes in Variably-Saturated Media, Version 3.0, HYDRUS Software Series 1, Department of Environmental Sciences, University of California Riverside, Riverside, CA, 270pp.
Small, E.E., 2005. Climatic controls on diffuse groundwater recharge in semiarid environments of the southwestern United States. Water Resour. Res. 41, W04012. http://dx.doi.org/10.1029/2004WR003193.
Taylor, R.G., Scanlon, B., Döll, P., et al., 2013. Ground water and climate change. Nat. Climate Change 3, 322–329.
van Genuchten, M.T., 1980. A closed-form equation for predicting the hydraulic conductivity of unsaturated soils. Soil Sci. Soc. Am. J. 44, 892–898.
Vogel, T., Dohnal, M., Dusek, J., Votrubova, J., Tesar, M., 2013. Macroscopic modeling of plant water uptake in a forest stand involving root-mediated soil water redistribution. Vadose Zone J. 12 (1).
Wang, T.J., 2014. Modeling the impacts of soil hydraulic properties on temporal stability of soil moisture under a semi-arid climate. J. Hydrol. 519, 1214–1224.
Wang, T.J., Zlotnik, V.A., 2012. A complementary relationship between actual and potential evapotranspiration and soil effects. J. Hydrol. 456, 146–150.
Wang, T.J., Zlotnik, V.A., Wedin, D., Wally, K.D., 2008. Spatial trends in saturated hydraulic conductivity of vegetated dunes in the Nebraska Sand Hills: effects of depth and topography. J. Hydrol. 349, 88–97.
Wang, T.J., Zlotnik, V.A., Šimunek, J., Schaap, M.G., 2009a. Using pedotransfer functions in vadose zone models for estimating groundwater recharge in semiarid regions. Water Resour. Res. 45, W04412. http://dx.doi.org/10.1029/2008WR006903.
Wang, T.J., Wedin, D., Zlotnik, V.A., 2009b. Field evidence of a negative correlation between saturated hydraulic conductivity and soil carbon in a sandy soil. Water Resour. Res. 45, W07503. http://dx.doi.org/10.1029/2008WR006865.
Wang, T.J., Istanbulluoglu, E., Lenters, J., Scott, D., 2009c. On the role of groundwater and soil texture in the regional water balance: an investigation of the Nebraska Sand Hills, USA. Water Resour. Res. 45, W10413.
Wesseling, J.G., 1991. Meerjarige simulatie van grondwaterstroming voor verschillende bodemprofielen, grondwatertrappen en gewassen met het model SWATRE, Wageningen. DLO-Staring Centrum, Rapport 152, 63.
Wood, E.F., Roundy, J.K., Troy, T.J., van Beek, L.P.H., Bierkens, M.F.P., Blyth, E., de Roo, A., Doll, P., Ek, M., Famiglietti, J., Gochis, D., van de Giesen, N., Houser, P., Jaffe, P.R., Kollet, S., Lehner, B., Lettenmaier, D.P., Peters-Lidard, C., Sivapalan, M., Sheffield, J., Wade, A., Whitehead, P., 2011. Hyperresolution global land surface modeling: meeting a grand challenge for monitoring Earth's terrestrial water. Water Resour. Res. 47, W05301.
Wösten, J.H.M., Pachepsky, Y.A., Rawls, W.J., 2001. Pedotransfer functions: bridging the gap between available basic soil data and missing soil hydraulic characteristics. J. Hydrol. 251, 123–150. http://dx.doi.org/10.1016/S0022-1694(01)00464-4.
Yokoo, Y., Sivapalan, M., Oki, T., 2008. Investigating the roles of climate seasonality and landscape characteristics on mean annual and monthly water balances. J. Hydrol. 357 (3), 255–269.
Zhang, L., Dawes, W.R., Walker, G.R., 2001. Response of mean annual evapotranspiration to vegetation changes at catchment scale. Water Resour. Res. 37, 701–708.
Zlotnik, V.A., Wang, T., Nieber, J.L., Simunek, J.A., 2007. Verification of numerical solutions of the Richards equation using a traveling wave solution. Adv. Water Resour. 30, 1973–1980.